Critical tests of stellar evolution in open clusters.
I. New photometry and radial velocities for NGC 3680*

B. Nordström, J. Andersen and M.I. Andersen

Niels Bohr Institute for Astronomy, Physics, and Geophysics, Astronomical Observatory, Juliane Maries Vej 30, DK-2100 Copenhagen, Denmark

Abstract. — We present new CCD photometry in the b and y colours of the Strömgren *uvby* system for 310 stars in a $13' \times 13'$ field centered on the intermediate-age open cluster NGC 3680. Careful cross-checks indicate that previously published *BV* photometry of NGC 3680 is affected by random and/or systematic errors precluding its use in critical comparison with theoretical isochrone computations. Detailed notes on several individual stars are given. In addition, we present ≈ 400 new photoelectric radial-velocity observations of 109 stars obtained with the CORAVEL scanner during the period 1988-1994. These data allow substantially complete identification of member and non-member stars in the field, and of spectroscopic binaries in both groups. Rotational velocities have also been derived for the programme stars, and our velocity variability criteria for stars of all rotations are described. The further astrophysical discussion of the data, including the definition of radial-velocity membership criteria, theoretical isochrone fitting, and the dynamical state of the cluster and the origin of its "bimodal turnoff", will appear in a separate paper (Nordström et al. 1996).

Key words: stars: evolution — stars: fundamental parameters — stars: HR diagram — stars: kinematics — open clusters and associations: NGC 3680

1. Introduction

Intermediate-age and old open star clusters are classic test objects in a variety of stellar and Galactic research fields. As ensembles of stars of identical age and chemical composition, star clusters are favourite test objects for stellar evolution models (e.g. VandenBerg 1983, 1985; Demarque et al. 1994). Clusters are also key objects in probing the structure and evolution of the galactic disk (e.g. Janes & Phelps 1994). With the increasing awareness of the complexities of the actual evolutionary history of the Galactic disk and its stars, demands on the quality and quantity of observational data are continually increasing.

Most investigations using cluster colour-magnitude diagrams (CMDs) rest on the basic, if sometimes implicit assumption that an accurate sequence of single cluster stars can be defined in a well-observed and well-calibrated CMD. Real CMDs, however, inevitably contain an admixture of field and binary stars which complicate the inter-

pretation; and photometry, whether photographic, photoelectric, or CCD, is not always perfect. Sparsely populated open clusters present special difficulties if the contrast from the field star background is low and binary stars are frequent.

Proper motion studies of sufficient accuracy are important to separate cluster and field stars, but still exist for only a handful of nearby clusters and leave close binaries undetected. In contrast, radial-velocity studies give information on both cluster membership and duplicity and do not require first-epoch plates. Radial-velocity data have already proved to be of considerable value in, e.g. M 67 (Mathieu & Latham 1986; Mathieu et al. 1986; Nissen et al. 1987) and NGC 752 (Daniel et al. 1994). This paper reports the first results of a program to provide such precise radial-velocity data and, where needed, new photometry for selected southern open clusters.

NGC 3680, the first object to be discussed in this program, is an intermediate-age (approx. 2 Gyr) cluster of metallicity slightly above solar (Eggen 1969; Nissen 1988 = N88). CCD *uvby* photometry of the central parts of NGC 3680 was published by Anthony-Twarog et al. (1989; ATTS), photoelectric *uvby*-H$_\beta$ photometry for 33 stars by N88, and CCD and photographic *BV* photometry in a large field centered on NGC 3680 by Anthony-Twarog et

al. (1991; AHTC). Very recently, a proper-motion study of the cluster was also published by Kozhurina-Platais et al. (1995).

Our comparisons between the photometric data from the above sources revealed a number of systematic and individual inconsistencies precluding their use for accurate comparison with theoretically computed isochrones. Therefore, we have obtained new CCD photometry in the Strömgren *uvby* system in a $13'\times13'$ field centered on NGC 3680. These results are reported and compared to previous photometry in the present paper (Sect. 2).

No radial-velocity study of sufficient accuracy to segregate cluster and field stars and detect the majority of spectroscopic binaries is available for NGC 3680, except for the recent survey of 15 red-giant candidates by Mermilliod et al. (1995). Accordingly, the bulk of our observational effort has been devoted to a radial-velocity survey of the cluster and the field in which it is imbedded. These data are also presented in the present paper (Sect. 3). With the new photometry, radial velocities, and proper motions, a comprehensive discussion of the cluster becomes possible, which is the subject of Paper II in this series (Nordström et al. 1996). Preliminary results from our radial-velocity survey were made available by us for the discussions in ATTS and AHTC (see also Nordström & Andersen 1991 and Andersen & Nordström 1991).

At present, no less than four different numbering systems exist for the stars in NGC 3680: That by Eggen (1969), identified here by the prefix E, the two different systems introduced by AHTC and ATTS (who give cross-references), and the numbering used in the proper-motion study by Kozhurina-Platais et al. (1995), who also give cross-references to Eggen and AHTC. For the brighter stars, Eggen numbers have been used most frequently in previous papers on NGC 3680; as the AHTC list was the most exhaustive available when the bulk of our observations were made, we have primarily used that to identify fainter stars and stars outside the field studied by Eggen.

Three close doubles were omitted by AHTC due to crowding, but resolved on the CCD frames of ATTS and ourselves; we have included them in the AHTC system by adding 4000 to their ATTS numbers (Nos. 6027, 6028, and 7020). A few close companions to stars with Eggen numbers have been discovered here and labelled with suffixes: 21B (a companion to 21A), 30A, and 59A. For the stars in our CCD frames for which no previous Eggen or AHTC numbers existed, we have assigned running numbers in order of increasing right ascension, adding 9000 to avoid overlap with the previous AHTC system.

Thus, a unified numbering system will be used in the remainder of this paper (see Table 1) and in Paper II: Numbers below 100 refer to Eggen (1969), between 1000 and 5000 to AHTC, between 6000 and 8000 to ATTS (subtract 4000 to get the ATTS numbers as published), and numbers above 9000 to the stars newly observed

in our CCD photometry. For convenience, Table 2 gives cross-references between this system and the numbers of Kozhurina-Platais et al. (1995) for stars measured in our radial-velocity survey.

Finally, with contemporary astronomical technology, accurate coordinates are more useful and less ambiguous stellar identifications than labelled finding charts. Accordingly, we have determined equatorial coordinates for all stars measured on our CCD frames, using all available stars from the HST Guide Star Catalog (Lasker et al. 1990) as reference stars. The resulting accuracy is about $0\overset{''}{.}4$, and comparison with stars in Kozhurina-Platais et al. (1995) shows agreement to better than $0\overset{''}{.}5$ in both coordinates. Stars in AHTC, but outside the CCD field, have been identified in the HST Guide Star Catalog, and coordinates for these stars are given at the end of Table 1.

2. Photometric data for NGC 3680

In preparation for the discussion of the CMD of NGC 3680, we performed a number of consistency checks on the published photometry for NGC 3680. The results of these checks (cf. Sect. 2.2 below) indicated that none of the existing photometry was both extensive and reliable enough to be useful in isochrone fitting at the intended level of precision. Therefore, new CCD photometry was obtained as described in the following.

2.1. *New CCD photometry*

New CCD photometry was obtained with the 1.54m Danish telescope on La Silla, on the night Jan. 25/26, 1995, using the wide field instrument Danish Faint Object Spectrograph & Camera (DFOSC; see Andersen et al. 1995a). DFOSC, which is a combined focal reducer and spectrograph, is equipped with a thinned 2048×2048, 15-μ pixel Loral CCD detector. With a QE above 70% in the whole spectral range $3000-8000$ Å, the response of the detector permits a good match to the standard filter-defined passbands. The final pixel scale is $0\overset{''}{.}391$ per pixel, giving a field of view of $13\overset{'}{.}35$. Thus, nearly the entire cluster itself and a good area of the surrounding field are covered by a single exposure.

On the night of observation, the weather was photometric and the seeing around $1\overset{''}{.}5$. In each of the b and y filters, ten 30-s. exposures and four 90-s. exposures were obtained. Between exposures, the telescope was offset by $3''$ to $3'$. Half of the exposures were obtained in one rotator position, the other half in the opposite rotator position. In each filter, six sky flats were obtained, covering both rotator positions.

All images were bias subtracted and flat field corrected by the combined sky flats, using IRAF[1]. In this generally

Table 1. Coordinates and CCD *by* photometry in the Ström-gren system for 310 stars in a 13′×13′ field centered on NGC 3680. For an additional 42 stars observed with CORAVEL, but outside the CCD field, coordinates from the HST GSC are listed at the end of the table

ID no.	α	(2000) δ	V	$(b-y)$
2006	11 26 07.6	-43 14 19.5	15.808	0.389
2015	11 26 13.5	-43 15 19.9	15.927	0.448
2016	11 26 09.6	-43 15 26.8	17.060	0.433
2017	11 26 06.5	-43 15 00.8	16.734	0.549
2018	11 26 05.9	-43 15 13.9	17.394	0.459
2019	11 26 03.3	-43 15 26.8	17.425	0.513
2020	11 26 02.1	-43 15 29.4	17.429	0.469
2021	11 26 01.5	-43 15 42.6	17.284	0.410
2023	11 25 49.7	-43 15 28.4	17.054	0.504
2024	11 25 48.5	-43 15 24.1	14.976	0.372
2025	11 25 44.3	-43 15 04.9	16.638	0.484
2026	11 25 40.3	-43 16 00.4	17.551	0.364
2028	11 25 48.3	-43 16 04.5	16.536	0.671
2029	11 25 47.3	-43 16 15.9	17.355	0.399
2030	11 25 59.3	-43 16 19.8	14.602	0.449
2031	11 26 01.9	-43 16 12.2	15.182	0.387
2032	11 26 02.3	-43 15 57.2	13.604	0.571
2033	11 26 06.0	-43 16 08.0	15.533	0.432
2046	11 26 12.3	-43 16 51.9	16.177	0.337
2048	11 26 04.5	-43 16 43.7	17.718	0.492
2049	11 26 02.1	-43 16 48.2	16.657	0.520
2051	11 25 45.2	-43 16 28.3	15.326	0.491
2052	11 25 44.7	-43 16 43.9	16.910	0.399
2054	11 25 40.4	-43 16 19.7	16.682	0.381
2055	11 25 40.4	-43 17 07.6	16.776	0.460
2057	11 25 45.0	-43 17 36.2	16.500	0.580
2058	11 25 46.9	-43 17 44.0	15.780	0.486
2059	11 25 46.3	-43 17 18.2	17.646	0.522
2060	11 25 54.4	-43 17 48.5	15.673	0.585
2061	11 25 53.7	-43 18 15.3	17.175	0.472
2062	11 26 07.9	-43 18 25.6	13.637	0.317
2063	11 26 02.2	-43 18 33.2	15.869	0.480
2064	11 26 06.1	-43 18 45.5	17.072	0.571
2065	11 26 07.1	-43 18 40.4	16.770	0.657
2067	11 26 12.2	-43 18 00.2	16.125	0.549
2081	11 26 11.9	-43 19 55.8	15.953	0.409
2082	11 26 10.9	-43 19 29.8	16.625	0.580
2083	11 26 07.1	-43 19 14.4	17.136	0.381
2084	11 26 06.7	-43 19 50.4	15.396	0.453
2085	11 26 08.7	-43 20 06.1	14.037	0.462
2089	11 26 02.8	-43 20 07.6	14.465	0.383
2090	11 25 57.7	-43 20 02.4	16.400	0.534
2091	11 25 55.7	-43 19 10.7	14.967	0.448
2092	11 25 50.6	-43 19 17.1	17.119	0.475
2093	11 25 51.8	-43 19 54.6	13.872	0.363
2095	11 25 45.8	-43 20 13.0	14.415	0.346
2096	11 25 42.8	-43 19 45.6	14.382	0.457
2097	11 25 43.8	-43 19 33.6	16.907	0.432
2098	11 25 47.0	-43 18 49.5	12.816	0.734
2099	11 25 46.7	-43 18 41.5	16.704	0.413
2100	11 25 41.2	-43 18 28.1	15.304	0.429
3001	11 25 37.0	-43 14 20.8	12.796	0.304
3002	11 25 30.6	-43 14 37.0	17.844	0.407
3008	11 25 06.6	-43 16 04.2	16.502	0.719
3009	11 25 18.9	-43 15 43.4	17.323	0.468
3015	11 25 37.3	-43 15 32.1	17.183	0.750
3016	11 25 36.9	-43 15 47.2	15.469	0.471
3018	11 25 36.4	-43 16 21.1	17.293	0.474
3019	11 25 31.7	-43 16 16.9	17.225	0.395
3020	11 25 30.8	-43 15 42.8	16.884	0.607

Table 1. continued

ID no.	α	(2000) δ	V	$(b-y)$
3022	11 25 26.7	-43 15 47.3	14.224	0.629
3023	11 25 24.7	-43 16 01.4	17.092	0.440
3024	11 25 21.0	-43 16 35.0	16.819	0.464
3026	11 25 12.7	-43 17 07.4	15.423	0.530
3027	11 25 08.3	-43 16 53.1	15.264	0.588
3043	11 25 05.6	-43 17 32.7	16.773	0.475
3044	11 25 03.8	-43 18 15.4	16.411	0.654
3045	11 25 05.3	-43 18 27.4	16.267	0.454
3046	11 25 08.4	-43 18 24.3	16.192	0.437
3047	11 25 11.8	-43 18 20.0	17.218	0.536
3049	11 25 24.1	-43 17 31.7	16.712	0.604
3050	11 25 22.8	-43 18 05.4	14.891	0.490
3051	11 25 23.0	-43 18 18.3	16.340	0.461
3053	11 25 33.3	-43 17 05.0	16.829	0.416
3054	11 25 36.7	-43 17 07.6	15.833	0.421
3055	11 25 36.2	-43 17 25.8	15.654	0.476
3057	11 25 33.6	-43 17 30.5	17.399	0.466
3063	11 25 12.7	-43 19 27.3	14.196	0.666
3064	11 25 07.9	-43 19 27.3	14.108	0.396
3072	11 25 13.2	-43 20 07.8	16.333	0.226
3074	11 25 15.3	-43 19 53.5	17.100	0.670
3077	11 25 22.6	-43 20 08.4	16.516	0.535
3078	11 25 31.8	-43 20 11.5	16.307	0.557
3079	11 25 36.7	-43 19 59.2	17.328	0.356
4002	11 25 38.0	-43 13 50.2	13.141	0.308
4005	11 25 38.1	-43 12 52.1	15.515	0.429
4009	11 25 25.1	-43 12 33.1	16.436	0.434
4011	11 25 16.8	-43 13 25.6	14.503	0.441
4013	11 25 12.3	-43 13 41.2	16.134	0.444
4014	11 25 11.9	-43 13 24.6	15.759	0.453
4015	11 25 11.3	-43 13 10.5	13.188	0.567
4016	11 25 10.4	-43 13 59.9	16.000	0.495
4017	11 25 02.7	-43 12 35.2	15.579	0.605
4018	11 25 03.0	-43 12 46.0	15.893	0.468
4031	11 25 02.2	-43 11 36.5	17.170	0.507
4032	11 25 02.6	-43 12 05.2	16.084	0.479
4034	11 25 07.6	-43 12 17.2	17.270	0.404
4035	11 25 13.7	-43 11 50.4	16.376	0.473
4037	11 25 20.8	-43 11 59.4	16.901	0.442
4038	11 25 19.6	-43 11 39.2	16.331	0.493
4039	11 25 16.4	-43 11 23.9	17.454	0.452
4040	11 25 14.7	-43 11 02.9	16.803	0.420
4041	11 25 19.8	-43 11 00.3	16.422	0.432
4042	11 25 22.5	-43 11 24.1	16.856	0.430
4044	11 25 26.0	-43 12 00.4	15.365	0.559
4045	11 25 28.4	-43 11 21.3	16.164	0.559
4046	11 25 30.1	-43 11 28.3	17.174	0.560
4047	11 25 29.9	-43 11 18.2	16.063	0.577
4048	11 25 30.1	-43 11 00.9	16.866	0.572
4050	11 25 32.9	-43 11 59.1	16.429	0.470
4051	11 25 40.1	-43 12 03.6	16.522	0.424
4052	11 25 37.2	-43 11 47.1	17.244	0.479
4054	11 25 35.8	-43 10 43.4	16.779	0.463
4055	11 25 35.7	-43 10 14.0	16.307	0.422
4058	11 25 27.7	-43 09 47.5	16.809	0.455
4059	11 25 30.7	-43 09 13.0	15.783	0.456
4060	11 25 26.8	-43 08 58.3	15.487	0.593
4061	11 25 25.9	-43 09 23.4	17.185	0.446
4062	11 25 24.2	-43 09 42.2	17.175	0.478
4063	11 25 23.9	-43 10 27.4	16.949	0.500

Table 1. continued

ID no.	α	(2000)	δ	V	$(b-y)$
4065	11 25 19.5	-43 10 10.4	16.860	0.486
4066	11 25 21.4	-43 09 52.8	16.448	0.473
4067	11 25 22.2	-43 09 19.1	16.436	0.650
4069	11 25 20.0	-43 09 10.5	17.651	0.462
4071	11 25 16.5	-43 10 13.8	16.887	0.602
4073	11 25 10.3	-43 10 43.0	16.301	0.559
4074	11 25 06.7	-43 10 32.6	16.151	0.491
4075	11 25 06.7	-43 10 26.0	17.096	0.647
4075	11 25 06.3	-43 11 11.3	17.314	0.416
4077	11 25 03.7	-43 10 51.7	16.743	0.430
4088	11 25 02.6	-43 07 56.8	13.846	0.505
4089	11 25 06.7	-43 08 44.5	16.507	0.445
4090	11 25 06.1	-43 09 37.5	16.848	0.475
4091	11 25 09.2	-43 09 21.1	15.137	0.466
4093	11 25 10.5	-43 07 41.0	15.165	0.377
4094	11 25 15.1	-43 07 44.4	11.858	0.579
4095	11 25 17.6	-43 08 30.9	14.770	0.463
4096	11 25 25.8	-43 08 41.3	16.860	0.775
4097	11 25 27.7	-43 08 27.2	17.027	0.538
4098	11 25 34.0	-43 08 36.3	17.478	0.450
4099	11 25 33.6	-43 08 00.7	16.026	0.720
4100	11 25 40.0	-43 08 29.0	15.477	0.361
4101	11 25 40.2	-43 08 02.2	14.933	0.441
4102	11 25 34.6	-43 07 10.2	17.192	0.679
4103	11 25 29.8	-43 06 59.6	14.806	0.409
4104	11 25 22.2	-43 07 13.7	15.839	0.849
4105	11 25 20.5	-43 07 28.3	17.318	0.418
4116	11 25 06.2	-43 07 14.9	13.959	0.415
6016	11 25 37.4	-43 14 18.2	16.736	0.501
6027	11 25 42.8	-43 13 38.6	12.026	0.353
6028	11 25 42.7	-43 13 41.0	12.648	0.297
7020	11 25 32.6	-43 15 50.9	14.266	0.485
7021	11 25 32.8	-43 15 47.4	15.839	0.519
9001	11 26 13.8	-43 18 46.8	18.051	0.435
9002	11 26 13.2	-43 13 59.1	17.841	0.452
9003	11 26 12.7	-43 11 56.1	17.376	0.453
9004	11 26 11.3	-43 11 34.5	17.744	0.448
9005	11 26 09.6	-43 13 37.6	15.302	0.353
9006	11 26 09.2	-43 08 26.9	17.772	0.736
9007	11 26 06.2	-43 19 36.0	17.896	0.808
9008	11 26 06.2	-43 18 19.7	17.661	0.580
9009	11 26 02.1	-43 12 13.5	17.467	0.635
9010	11 25 57.8	-43 19 40.4	17.854	0.767
9011	11 25 56.3	-43 13 08.6	16.621	0.537
9012	11 25 54.3	-43 07 32.1	17.598	0.539
9013	11 25 53.4	-43 07 51.6	17.660	1.008
9014	11 25 53.0	-43 14 35.9	17.293	0.434
9015	11 25 50.6	-43 09 02.7	17.245	0.642
9016	11 25 49.7	-43 17 52.4	17.626	0.648
9017	11 25 49.5	-43 09 24.0	17.673	0.641
9018	11 25 48.5	-43 08 14.7	17.354	0.828
9019	11 25 47.5	-43 17 05.2	17.595	0.461
9020	11 25 43.0	-43 18 56.8	17.770	0.442
9021	11 25 39.2	-43 16 13.3	17.551	0.577
9022	11 25 33.8	-43 19 01.1	18.101	0.368
9023	11 25 24.2	-43 19 27.4	17.848	0.532
9024	11 25 23.8	-43 10 59.5	17.243	0.929
9025	11 25 22.8	-43 16 03.5	17.665	0.656
9026	11 25 20.9	-43 13 21.5	17.550	0.617
9027	11 25 19.8	-43 11 54.7	16.748	0.697

Table 1. continued

ID no.	α	(2000)	δ	V	$(b-y)$
9028	11 25 19.1	-43 15 46.7	17.360	0.499
9029	11 25 18.6	-43 17 17.1	17.020	0.733
9030	11 25 18.0	-43 14 46.7	17.681	0.583
9031	11 25 17.4	-43 11 12.2	18.185	0.538
9032	11 25 16.0	-43 18 04.5	17.626	0.531
9033	11 25 15.2	-43 16 37.3	17.999	0.487
9034	11 25 13.3	-43 14 18.0	17.848	0.604
9035	11 25 13.1	-43 17 04.0	17.465	0.483
9036	11 25 11.7	-43 18 40.0	17.740	0.656
9037	11 25 08.3	-43 19 35.2	17.488	0.723
9038	11 25 07.9	-43 11 46.7	17.665	0.600
9039	11 25 07.3	-43 18 36.2	17.708	0.656
9040	11 25 06.7	-43 12 58.6	17.572	0.513
9041	11 25 02.4	-43 09 11.9	17.218	0.774
1	11 25 01.5	-43 10 23.4		
3	11 25 00.0	-43 15 24.0		
50	11 26 24.8	-43 15 25.8		
53	11 26 36.4	-43 15 14.5		
54	11 26 39.7	-43 14 43.3		
55	11 26 41.5	-43 10 18.8		
60	11 26 20.7	-43 13 08.0		
61	11 26 21.2	-43 13 30.8		
62(A)	11 26 33.4	-43 22 32.6		
63(B)	11 26 41.1	-43 21 17.5		
64(C)	11 26 38.9	-43 21 08.3		
65(D)	11 26 40.3	-43 18 17.6		
66(E)	11 26 49.6	-43 17 35.4		
67(F)	11 26 52.7	-43 11 45.2		
68(G)	11 26 50.2	-43 11 35.9		
69(H)	11 24 58.5	-43 16 27.8		
76(P)	11 24 46.0	-43 12 31.7		
77(Q)	11 26 41.6	-43 15 27.1		
78(R)	11 24 55.7	-43 06 10.7		
1079	11 26 29.1	-43 07 34.3		
1083	11 26 15.5	-43 07 50.7		
1124	11 26 00.8	-43 05 31.8		
2040	11 26 32.7	-43 16 32.9		
2076	11 26 21.2	-43 20 30.9		
2094	11 25 46.3	-43 20 30.0		
2110	11 26 10.2	-43 21 59.4		
2117	11 26 33.8	-43 23 32.9		
2118	11 26 27.0	-43 23 29.2		
2125	11 26 13.0	-43 23 27.7		
3028	11 25 01.3	-43 16 37.4		
3040	11 25 00.8	-43 18 25.3		
3095	11 24 58.6	-43 22 53.2		
3104	11 25 19.7	-43 22 28.3		
3105	11 25 19.8	-43 22 41.3		
3113	11 25 36.9	-43 22 33.9		
4027	11 24 47.6	-43 12 21.2		
4028	11 24 48.3	-43 12 18.1		
4081	11 24 51.1	-43 09 16.2		
4106	11 25 26.8	-43 05 58.1		
4114	11 25 11.6	-43 06 31.5		
4121	11 24 53.0	-43 06 34.5		
4140	11 25 36.5	-43 05 00.1		

quite uncrowded field, aperture photometry for aperture radii of 4, 5, 6, 7 and 8 pixels was derived for individual frames, using IRAF/APPHOT. The flat field errors were determined by the method described by Andersen et al. (1995b). Briefly, the magnitude differences for individual stars between offset and rotated exposures are used to determine a global fit to the flat field error. After applying this correction to the flat field, the 6-pixel aperture was identified as giving the best overall results, with a typical internal error of $0\overset{m}{.}014$, independent of magnitude down to $V=15\overset{m}{.}5$.

Due to significant PSF variations across the field, the DAOPHOT package for PSF photometry (Stetson 1987) is not suitable as a general method. In a few cases, however, blended images of close doubles caused problems. For stars with faint, close companions (star pairs E30/30A, E47/47A, E59/59A, E21A/21B, and 6027/6028), the fainter stars were first subtracted with DAOPHOT/SUBSTAR. Aperture magnitudes were then redetermined from 3 frames. From the deduced magnitude offset to the previous aperture photometry, precise determinations of the contribution from the fainter components were made. Subsequently, the magnitudes of the fainter companions were determined by DAOPHOT/PSF photometry within each pair. In doing this, we only need to assume that PSF photometry is reliable over small areas where PSF variations are small.

The close bright pair 6027/6028 is a special case. Here, a large aperture (20 pixels radius) was used to determine the total magnitude of the pair relative to stars E32, E33, and E38, after subtracting all other stars from the frames. Their individual magnitudes were then derived, using the difference in PSF magnitude. Our final photometry in the instrumental system was formed as the average of the magnitudes measured from the individual images.

We have 29 stars in common with the photoelectric $uvby$-H$_\beta$ photometry of N88, two of which (E21A and E30) are now identified as visual binaries. The remaining 27 stars were used to derive the standard transformation. Since the observations were made in rapid succession and the standard stars are located in the same field, extinction correction can be simply incorporated in the colour transformation.
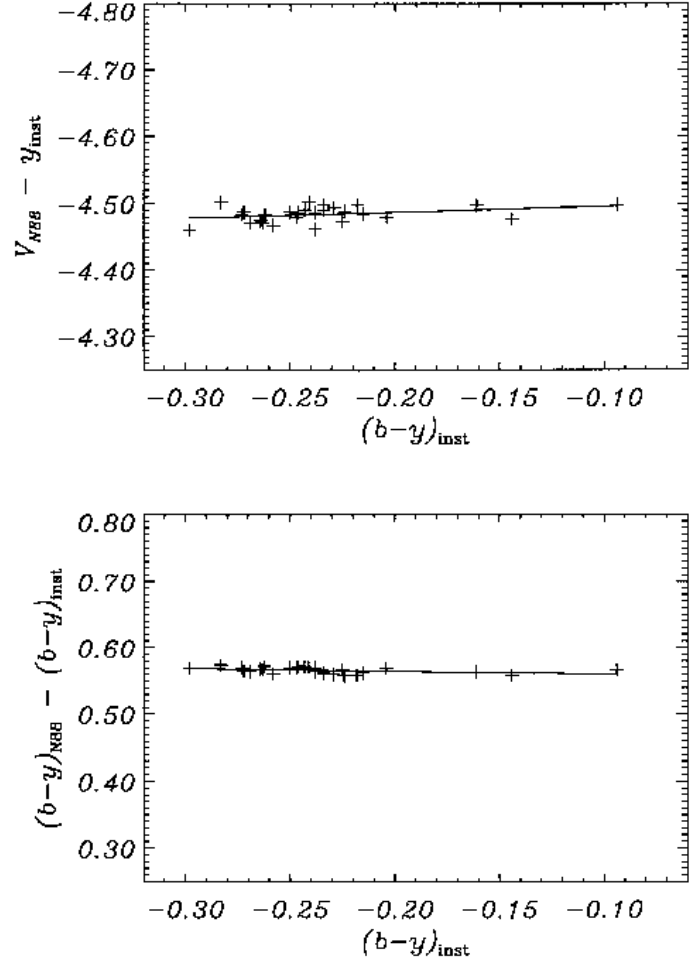
Using the procedure of Grønbech et al. (1976), we derived the following standard relations (see Fig. 1):

$$V_{\mathrm{std}} = y_{\mathrm{inst}} - 0.089(b-y)_{\mathrm{inst}} + \mathrm{constant} \qquad (1)$$

$$(b-y)_{\mathrm{std}} = 0.955(b-y)_{\mathrm{inst}} + \mathrm{constant} \qquad (2)$$

The reduced standard deviation in $(V_{\mathrm{NAA}} - V_{\mathrm{N88}})$ and $((b-y)_{\mathrm{NAA}} - (b-y)_{\mathrm{N88}})$ is $0\overset{m}{.}0114$ and $0\overset{m}{.}0044$ respectively. N88 lists standard errors as function of magnitude,

[1]IRAF is developed and distributed by NOAO.

Fig. 1. a-b. Plots of the V magnitude and $(b-y)$ colour transformations from our CCD instrumental system to N88, using the same scale as in Fig. 3

from which we deduce average standard errors of $0\overset{m}{.}0064$ and $0\overset{m}{.}0047$ in V and $(b-y)$ respectively. Assuming that the errors are uncorrelated, a standard error of $0\overset{m}{.}0094$ in V is derived for our data. In $(b-y)$ we are in the unusual, but statistically possible situation that the error derived from the comparison with N88 is smaller than the internal error in the N88 data. The standard errors in N88 are derived from repeated observations of ≈ 200 stars and can therefore be considered as well determined. Given this, we can set an upper limit on our standard error in $(b-y)$ of $0\overset{m}{.}0034$ at the 90% confidence level.

It is appropriate to note, however, that since the N88 photometry covers only the main-sequence and turnoff region of the CMD, our photometry cannot be claimed to have been properly standardised in the red-giant region of the CMD. The same comment presumably applies to the ATTS photometry.

The final CMD for our full $13' \times 13'$ field surrounding NGC 3680, as constructed from our CCD photometry, is shown in Fig. 2.
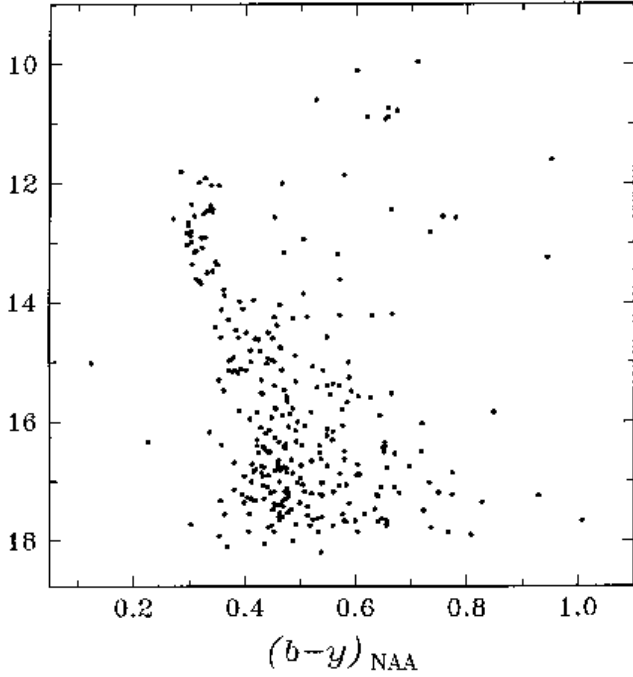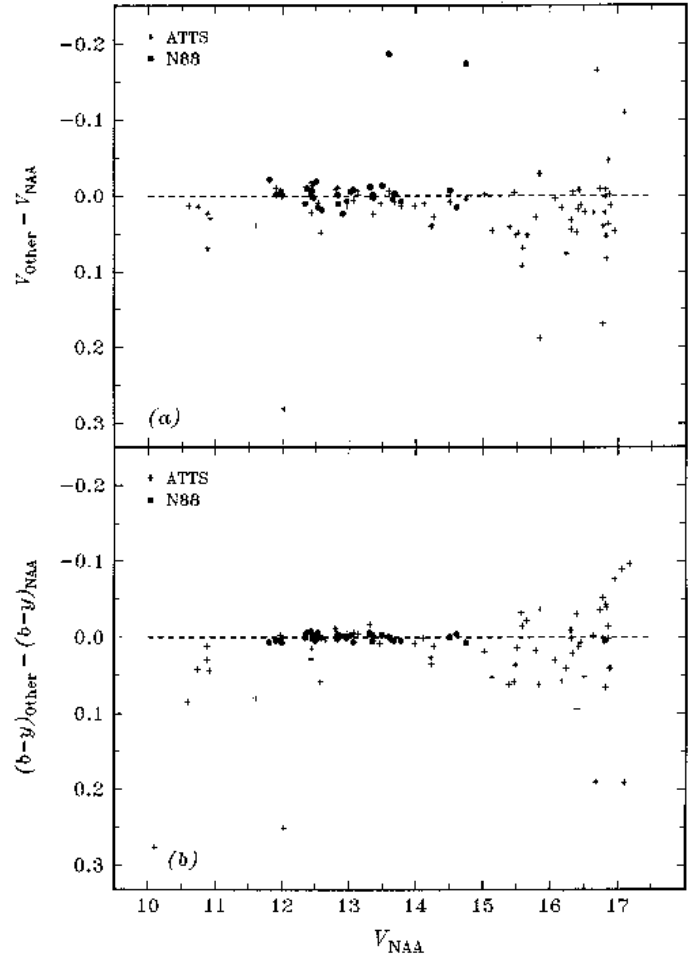

Fig. 2. Colour-magnitude diagram in the Strömgren system for all stars observed by us (NAA) in the field of NGC 3680

Fig. 3. V magnitude and $(b-y)$ colour differences between our CCD data (NAA) and those by N88 (dots) and ATTS (plusses) vs. magnitude; the two discrepant stars from N88 are the close doubles E21A and E30

2.2. *Previous photometric data for NGC 3680*

We recall that the sources of $(U)BV$ photometry for NGC 3680 are Eggen (1969) and AHTC (photographic photometry calibrated by photoelectric and CCD standard observations). In the $uvby$-H_β system, we have N88 (photoelectric photometry), ATTS (PSF-fitting CCD photometry), and the CCD aperture photometry reported above (NAA; b and y filters only). Since most theoretical isochrone calculations predict only broad-band colours as the directly observable parameters, it would be convenient to use the published BV data. Before proceeding to do so, we have compared the photometry from all the above sources in order to detect any systematic trends as well as individual discrepancies for the stars in common between them.

Since both sets of *uvby* CCD photometry were calibrated using the stars in N88, it is to be expected that both V and $(b-y)$ agree very well between those three papers, as functions of both magnitude and $(b-y)$ colour (Figs. 3 and 4). The exceptions are the close doubles E21A and E30 which, as mentioned above, were resolved by ATTS and by us, but not in the classical diaphragm photometry of N88, and E38 for which there seems to be a problem with the ATTS value of m_1. In addition, the ATTS value of $(b-y)$ for the red-giant binary E20, which

was not observed by N88, appears, for unknown reasons, to be some $0\overset{m}{.}20$ too large. The rms differences (ATTS-N88) for the remaining 17 stars in common are: $0\overset{m}{.}010$ (V), $0\overset{m}{.}007$ ($b-y$), $0\overset{m}{.}009$ (m_1), and $0\overset{m}{.}026$ (c_1). Except for c_1, these are in satisfactory agreement with the published error estimates. Our photometry and N88 were compared in Sect. 2.1.

In the BV photometry for NGC 3680 we do, however, find significant systematic differences between the different sources, far exceeding the quoted mean errors. Figures 5-7 summarise the comparisons we have made. Omitting star E20, the AHTC V magnitudes are systematically $0\overset{m}{.}06$ fainter than those determined here (and by ATTS and N88) for the 248 stars in common, with an rms difference of $0\overset{m}{.}04$ (Fig. 5). The Eggen V magnitudes are on average $0\overset{m}{.}09$ fainter than ours, with an rms dispersion of $0\overset{m}{.}09$, based on 53 stars and omitting stars E17, I, P, and R, which show very large discrepancies (Fig. 5).
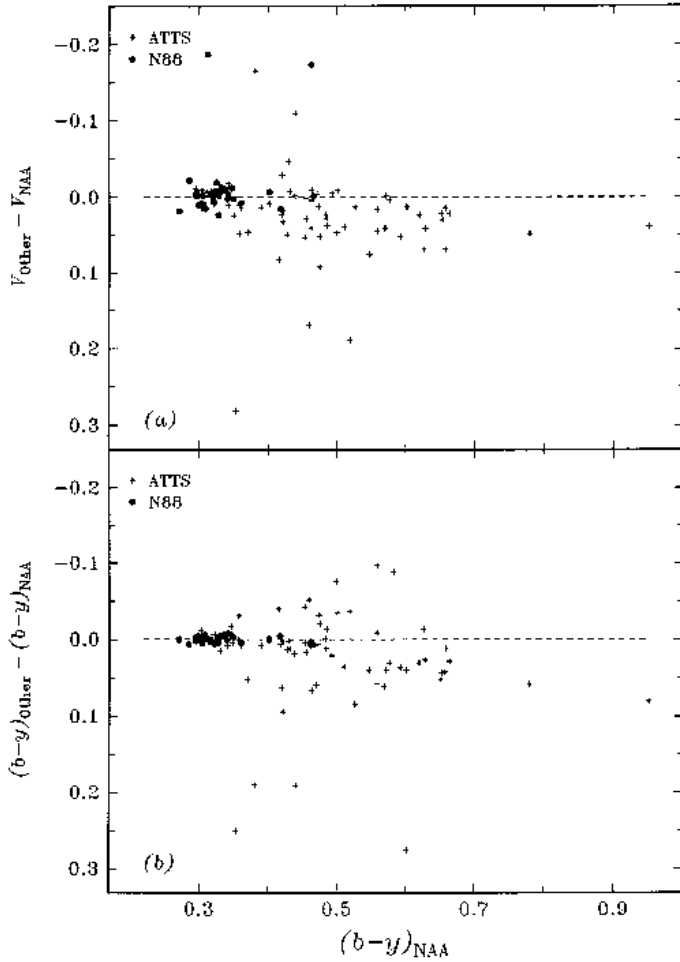
Fig. 4. V magnitude and $(b-y)$ colour differences between our CCD data (NAA) and those by N88 (dots) and ATTS (plusses) vs. $(b-y)$ colour index
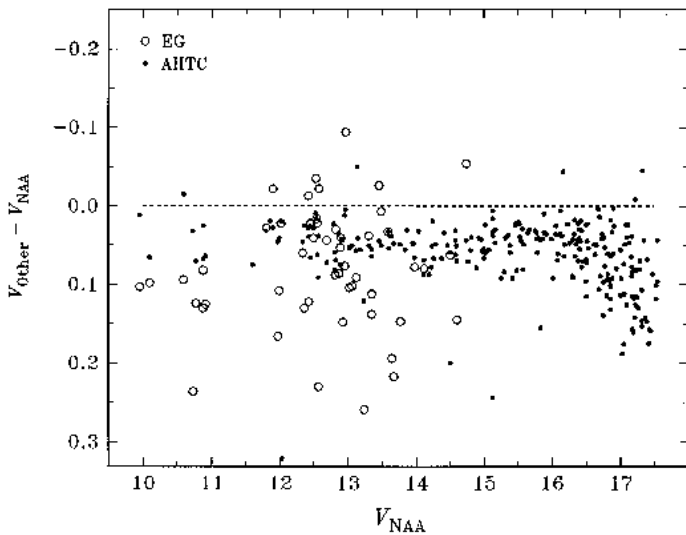

Fig. 5. V magnitude differences between our data (NAA) and those by Eggen (circles) and AHTC (dots) vs. magnitude
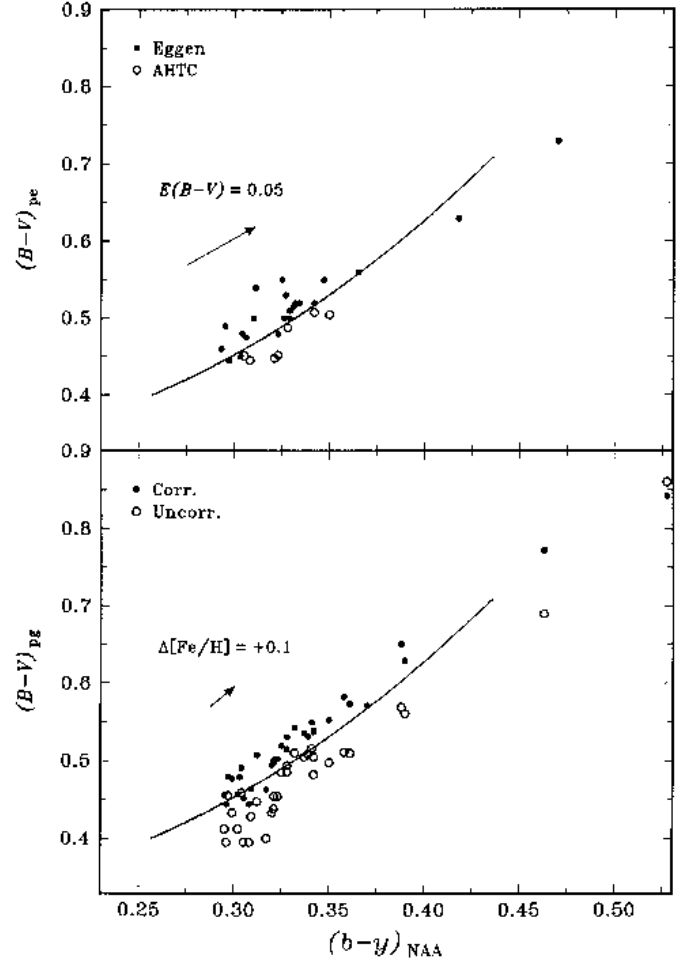
Fig. 6. Relation between the observed $(b-y)$ and $(B-V)$ colours for the radial-velocity members of NGC 3680. Upper: Photoelectric $(B-V)$ data. Lower: Photographic $(B-V)$ data from AHTC, both corrected as described in the text (dots) and directly as published (circles). The full line is the Hyades standard relation, reddened in both colours by the amounts observed for NGC 3680. Reddening and blanketing vectors appropriate to NGC 3680 are also shown

The systematic differences in $B-V$ between Eggen and AHTC, discussed extensively by AHTC, are illustrated in Fig. 7, which shows the difference between the (photoelectric) Eggen $(B-V)$ colours and the (photographic) $(B-V)_{\rm AHTC}$ data as published (circles). The large size and peculiar average trend of these differences as a function of $B-V$ itself led us to investigate the likely origin of these differences in more detail by plotting $(B-V)_{\rm AHTC}$ against $(b-y)$ for the main-sequence and turnoff stars in NGC 3680 (Fig. 6). Since the two clusters have the same metal abundance, the stars in NGC 3680 should fall on the Hyades relation, appropriately reddened in both colours. Accordingly, we plotted the Hyades standard main-sequence relation from Crawford & Perry (1966) in the same diagram, reddened by $E(b-y) =$

0.036 as found for NGC 3680 (N88) and, correspondingly, $E(B-V) = 0\overset{m}{.}050$.
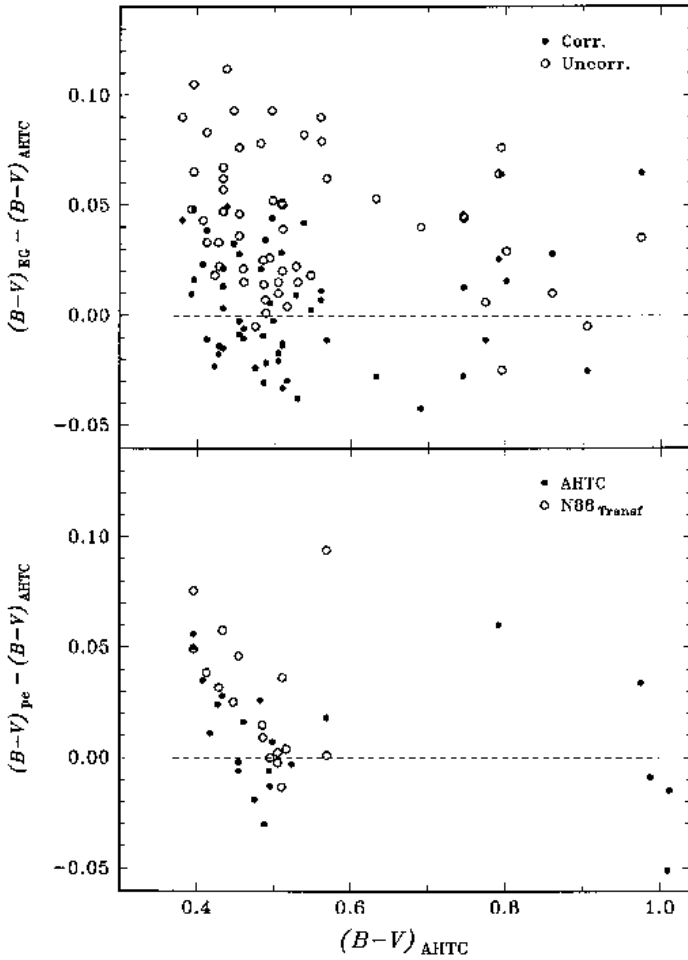
Fig. 7. Differences between the AHTC $(B-V)$ colours and other sources, vs. the published photographic $(B-V)_{\text{AHTC}}$. Upper: Photoelectric $(B-V)$ data from Eggen *minus* $(B-V)_{\text{AHTC}}$, both corrected (dots) and as published (circles). Lower: Photoelectric $(B-V)$ values from AHTC (their Table 3; dots) and from $(b-y)_{\text{N88}}$ as transformed to $(B-V)$ (circles), *minus* $(B-V)_{\text{AHTC}}$, vs. $(B-V)_{\text{AHTC}}$

Figure 6 shows that the expected agreement is manifestly not observed, neither for the photoelectric $(B-V)$ data by Eggen and later additional observations by AHTC (Fig. 6, upper panel), nor for the photographic data published by AHTC (lower panel). While most cluster stars near $(B-V)_{\text{AHTC}} = 0.5$ (circles) do lie near the reddened Hyades relation, most stars either redder or bluer than this have $(B-V)_{\text{AHTC}}$ values that are some $0\overset{m}{.}04-0\overset{m}{.}05$ too blue for their $(b-y)_{\text{N88}}$. Reddening and blanketing vectors appropriate to NGC 3680 are shown in the upper and lower panels of Fig. 6 and indicate that errors in the assumed reddening or metal abundance of the cluster cannot cause the observed discrepancies. One is led to regard

the published observational errors of the BV photometry with considerable reservation.

Based on past experience, we assume that the N88 photometry for the individual uncrowded stars and thus the derived mean reddening and metallicity are substantially correct. The deviations from the Hyades relation seen in Fig. 6 would then be interpreted as a systematic error in the AHTC BV photometry.

As a further check on this conjecture, we have drawn on such other photoelectric $(B-V)$ values as are available in addition to those by Eggen (1969). These are, first, the stars (re)observed by AHTC for calibration purposes (their Table 3; dots). Second, some independent values were obtained by transforming the N88 $(b-y)$ data to $(B-V)$ via the Hyades relation (Fig. 6), with appropriate reddening corrections. The differences of these transformed $(B-V)$ values from $(B-V)_{\text{AHTC}}$ have been added to the diagram in Fig. 7 (circles). As these independent and more recent photoelectric data show roughly the same form of systematic deviations from $(B-V)_{\text{AHTC}}$ as the Eggen observations, it would again appear that their origin lies in the standardization problems encountered by AHTC.

We must conclude that the published BV photometry for NGC 3680 is not accurate enough for our main purpose, a precise observational test of theoretical isochrone calculations. The strong deviation of the bluest main-sequence stars from the Hyades relation is particularly disconcerting, since these stars define the turnoff point, while the main-sequence termination point occurs near $(B-V)_{\text{AHTC}} = 0.5$, where the stars do fall closer to the Hyades relation. Thus, not only does the turnoff colour of NGC 3680 (hence, its age) become uncertain, but the entire shape of the turnoff itself, one of the key diagnostics of the computed isochrones, becomes strongly distorted.

This conclusion, combined with the lack of *uvby* data for many of the stars in the field, led us to redetermine the CMD of NGC 3680 in the *uvby* system as reported above, and the comparisons with theoretical isochrones in Paper II will be made primarily using these data.

However, in response to a draft of this paper, Drs. Anthony-Twarog and Twarog kindly re-examined the calibration of their photographic observations in considerable detail. They found that, apart from a small offset (see Fig. 5), their V magnitude scale is substantially correct as published, certainly so for stars brighter than $V = 15.5$. However, the B magnitude calibration turns out to contain a non-linearity which the previously available body of calibration stars had been inadequate to reveal. This non-linearity propagates directly into the $(B-V)$ colours since magnitude and colour are related for the cluster stars. Drs. Anthony-Twarog and Twarog recommend the following correction formula for their published photographic $(B-V)$ colours:

$$(B - V)_{\mathrm{corr}} = 0.98 \, (B - V)_{\mathrm{AHTC}} + 0.023 \, V_{\mathrm{AHTC}} - 0.244 \tag{3}$$

The corrected $(B-V)$ values are shown (as dots) alongside the published data in Figs. 6 (lower panel) and 7 (upper panel). The agreement with the Hyades relation, and especially with the Eggen $(B - V)$ colours, is clearly improved. However, systematic and random uncertainties of a few hundredths of a magnitude appear to remain, more than desirable for the detailed examination of the shape of the turnoff region of the cluster sequence which is the primary objective of this study (see Paper II).

Still, for consistency checks, for the red giants for which the by photometry cannot be properly calibrated using the F stars from N88, and when stars outside the CCD field are considered, we will occasionally make use of the AHTC BV photometry, and then with the corrections described above.

3. Radial-velocity data for NGC 3680

3.1. Observations

Radial-velocity observations of NGC 3680 were made with the photoelectric scanner CORAVEL, attached to the Danish 1.5-m telescope at ESO, La Silla, during several observing periods from January 1988 through January 1994. CORAVEL, its accuracy and radial-velocity zeropoint are discussed by Baranne et al. (1979), Mayor (1985) and Mayor & Maurice (1985). The observing list contained all 118 stars in the AHTC field around NGC 3680 which were potentially observable with the fixed K2 III mask of CORAVEL, i.e. all stars brighter than $B \approx 15.2$ and redder than $B - V \approx 0.38$. The red giants in NGC 3680 were also observed in order to define the mean radial velocity and velocity dispersion of NGC 3680; these data were recently published together with those on the red giants in the "sister cluster" of NGC 3680, IC 4651 (Mermilliod et al. 1995) and will, therefore, not be discussed further here. The present study is directed primarily at the main sequence and turnoff regions of NGC 3680, which are the crucial features of the CMD for determining the distance and age of the cluster, and for testing stellar models with different convection prescriptions.

Our observing strategy was designed with the primary aim to define a clean sample of single member stars in NGC 3680 from among the binaries and/or nonmembers. To this end, we have attempted to secure four or more observations, distributed over at least three years, for all candidate radial-velocity and/or photometric members of NGC 3680. A CMD of the complete sample of stars observed in the field of NGC 3680 is shown in Fig. 8 (BV data from AHTC).

Due to the difficulty of locating individual binary components correctly in the CMD, even if membership is supported by a systemic velocity derived from a full orbital
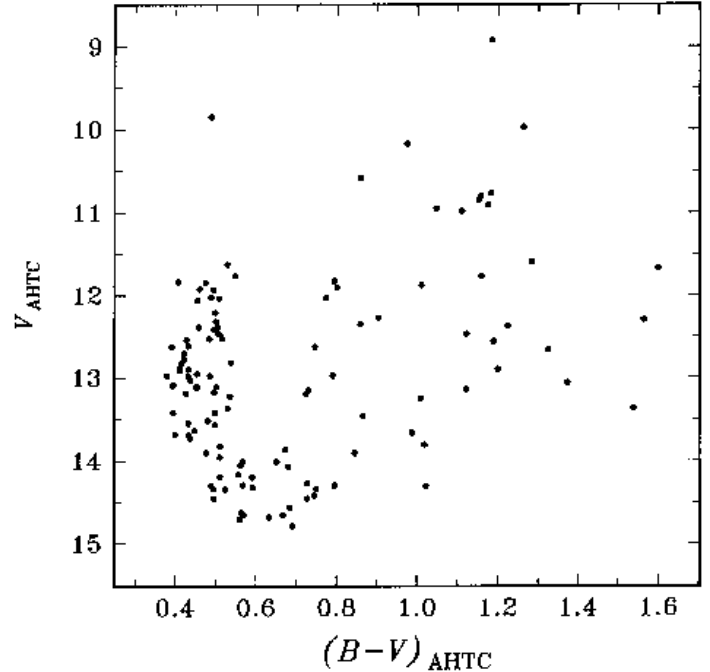
Fig. 8. BV colour-magnitude diagram (AHTC data) of all stars observed with CORAVEL in the AHTC field around NGC 3680

solution, we have not at this stage pursued the observation of suspected binary stars much beyond the point of unambiguous variability detection. Similarly, if two concordant observations classified a star as a non-member, we have not expended inordinate extra effort in a search for possible low-level variability. In all, about 400 observations were obtained on the program from January 1988 through January 1994.

3.2. Data reduction

A note on the reduction of the measurements is in order, because the important turnoff region in NGC 3680 contains stars that are near the upper limits in both temperature and rotation for stars to be observable with CORAVEL. At the same time, unambiguous separation of cluster and field stars places strict demands on the accuracy of the observed radial velocities.

As detailed by Baranne et al. (1979) and Mayor (1985), the cross-correlation profile is recorded directly in 40 or 64 points by CORAVEL. The radial velocity is determined by fitting the position, depth, and width of a Gaussian profile plus a continuum level to these data. For a single, constant star, the profile parameters derived from a single observation are more or less precise estimates of the true values, depending on the (photon) noise level of each data set. For observations with count levels significantly below average the fitted profile may deviate drastically from the rest, especially for fast-rotating stars. In these cases, it

is preferable to fix the profile shape parameters to their
weighted mean value over all well-integrated observations
of that star, leaving only the peak position (i.e. radial
velocity) and continuum level as free parameters in the fit.
Similarly, in double-lined binaries, the profile shapes are
fixed to their mean values from those observations where
the profiles are resolved.

3.3. Rotational velocities

From the width of the observed Gaussian cross-correlation
profiles, rotational velocities can be computed following
Benz & Mayor (1981, 1984). Thus, mean rotational veloc-
ities ($v\sin i$, with errors) have been determined for all the
programme stars. For some sharp-lined stars only an up-
per limit to $v\sin i$ could be determined, due to the finite
S/N of the profiles; no error estimate is then given. Be-
cause CORAVEL is optimized for observations of sharp-
lined, late-type stars, both rotational and radial velocities
become relatively uncertain for $v\sin i > 30-40$ km s^{-1}.

3.4. Results

Altogether, some 400 new radial-velocity observations
have been obtained of 118 main-sequence, turnoff, and
field stars in the $20' \times 20'$ field around NGC 3680 for which
photometry was obtained by AHTC. Table 2 lists weighted
mean radial and rotational velocities, with standard er-
rors, for 109 of these stars, determined as described above,
together with additional data on the observations and
notes on duplicity, etc. A few stars were found to be
too hot and/or too fast-rotating to yield a measurable
cross-correlation signal with CORAVEL, viz., E42, E55,
69(H), 72(K), 78(R), and AHTC 1094, 2030, 2110, and
6027 (ATTS 2027). For completeness, together with the
new rotational data, we include the red-giant radial veloc-
ities from Mermilliod et al. (1995), identified by remark
"M" in Table 2. The individual radial-velocity observa-
tions of the new stars, some of which might still turn out
to be binaries if monitored over a long period, are given
in Table 3 (only available in electronic form, see footnote
at the beginning of the paper).

A histogram of the observed radial velocities (Fig. 9)
leaves no doubt as to the existence of a real concentra-
tion of stars near the mean velocity of NGC 3680 itself,
0.87 km s^{-1} as determined from the six constant-velocity
red giants (Mermilliod et al. 1995). It also illustrates, how-
ever, that of the order of 8 field stars can still be expected
in the 5 km s^{-1} velocity bin centered on the cluster. The
detailed identification of these stars will be discussed in
Paper II.
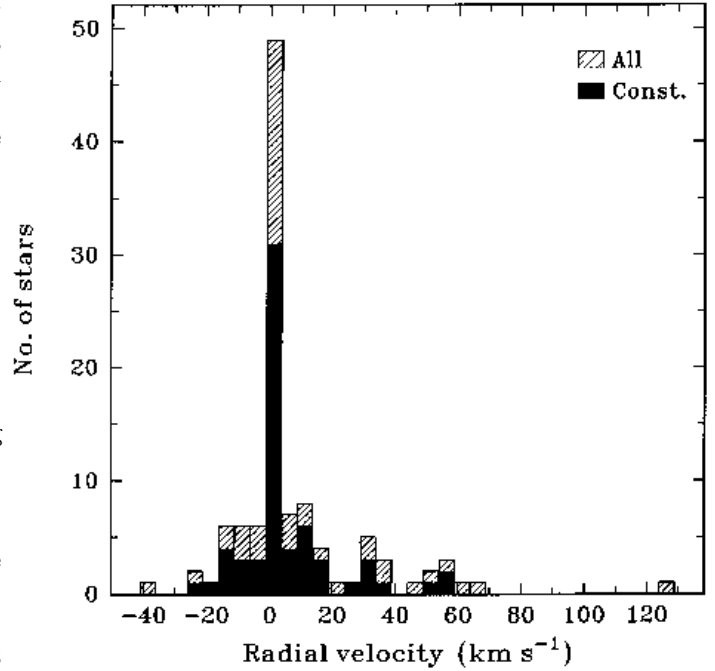
Fig. 9. Histogram of the observed radial velocities from Table
2, highlighting the stars judged to be constant from two or
more observations

3.5. Notes on individual stars

Asterisks in Table 2 identify stars on which separate com-
ments are given in the following (see also Mermilliod et
al. 1995 for specific comments on the red giants):

E1 is a double-lined binary with a large luminosity
ratio; the secondary has $v\sin i < 10$ km s^{-1}.

E11, a red giant, shows velocity variations at a low
level, but with high significance. It is some $0.^{\rm m}05$ bluer
in $(B - V)$ than the clump and probably has an upper
main-sequence companion.

E14 is a spectroscopic binary with components of
slightly different luminosity; the secondary has $v\sin i =
10 \pm 15$ km s^{-1}.

E18 is a short-period single-lined spectroscopic binary
and non-member (Mermilliod et al. 1995).

E20 and 34 were noted as probable giant binaries by
AHTC, being much brighter and bluer than the other
clump stars. Both are radial-velocity members and E20
indeed a textbook double-lined binary (Mermilliod et al.
1995). Surprisingly, ATTS found E20 to be far *redder* than
the clump and a probable photometric nonmember, sug-
gesting a problem with their CCD data for this star.

E21 is an F star with $(b - y) = 0.40$ from both ATTS,
N88, and our data, and a normal CORAVEL profile for
that colour. AHTC give $(B - V) = 2.35$, which must be a
misprint.

E21A and 30 are close double stars. They were omit-
ted by AHTC, and the N88 *uvby* photometry refers to the

combined light. The stars are resolved in PSF-fitting photometry, as noted in Sect. 2.1. Removing the light of the companions moves these stars downwards and to the blue in the cluster CMD relative to the positions shown by N88.

E22 is a double-lined binary with near-equal components; the secondary has $v\sin i = 10.6 \pm 2.9$ km s^{-1}.

E27, a red giant, is an unambiguous velocity variable, but is located precisely together with the single clump giants. A faint, late-type main-sequence companion would be consistent with these observations.

The red giant E34 in the center of NGC 3680, although not significantly variable in velocity during the 10-year period covered by the CORAVEL observations, has a cross-correlation profile only about half as deep as the other cluster giants. As it is also significantly bluer than the bulk of the red giants, we conclude that it has a blue, upper main-sequence or turnoff companion in a long-period and/or low-inclination orbit.

E36 is a double-lined binary; the secondary has $v\sin i = 9.1 \pm 3$ km s^{-1} (estimated error for both components).

E38 was considered metal-poor by ATTS on the basis of its m_1 index, but normal by N88 and AHTC. We include it in our sample of normal stars.

The red giant E41 was found by ATTS to have an anomalous m_1 index and be a likely non-member. It has constant radial velocity equal to the cluster mean, and a cross-correlation profile and $(B-V)$ index just like the other clump giants. Given no other evidence of peculiarity, we consider it to be a normal, single cluster member.

E62(A) is a double-lined binary with a sharp-lined primary; the secondary has $v\sin i = 22.5 \pm 3.4$ km s^{-1}.

4094, the single photometric lower giant-branch candidate, is a marginal radial-velocity member. As discussed by AHTC, 4094 may be the star actually observed by Eggen (1969) under the name of E17, rather than the star so identified on his chart.

6016 (ATTS 2016) is one of two stars identified as AHTC 3001 in ATTS. Consistent with the AHTC chart, we have retained the number 3001 for the brighter of the two stars close to the central red giant E34, while 6016 is its faint close companion.

6027/6028 (ATTS 2027/2028) is another close pair resolved by ATTS and us, and observable separately with CORAVEL in good seeing. For 6027, which has a fairly red $(b-y)$ colour and unusual m_1 index in the ATTS photometry, we find a much bluer $(b-y)$ which may explain why (like E55) it shows no correlation peak with CORAVEL. 6028 is confirmed as a (double-lined) cluster binary as predicted by AHTC; the secondary component has $v\sin i = 5.5$ km s^{-1}(upper limit).

4. Spectroscopic binary detection

From each observed CORAVEL profile, the predicted standard error can be computed. This error estimate (σ_C) is a function of the observed count level, profile shape,

and integration time (scintillation noise) as described in more detail by Mayor (1985), Andersen et al. (1985), and Duquennoy & Mayor (1991).

From the observed and computed errors, we can compute the value of χ^2 for each star and the probability $P(\chi^2)$ that it could arise purely due to random errors. When that probability is less than 1%, the star is classified as a probable binary; otherwise, the default hypothesis of a constant-velocity, single star is retained. Stars found to be constant on the basis of two or more observations and on this criterion are highlighted in Fig. 9.

For reliable results, this procedure clearly requires that σ_C is correctly estimated. If this condition is satisfied, the ratio O/C between observed standard deviation (σ_E) and computed error (σ_C, mean value) should average unity for constant stars, regardless of, e.g. rotation. However, in early F-type stars such as the turnoff stars in NGC 3680, rotational broadening is in fact the most serious impediment to obtaining accurate radial velocities: Indeed, no useful data at all could be obtained for a few stars, as noted above (Sect. 3.4). As the profile width enters significantly in the calculation of the expected error, but is poorly determined in very shallow profiles, it is important to check whether our variability criterion is adequate and consistent for all rotations.
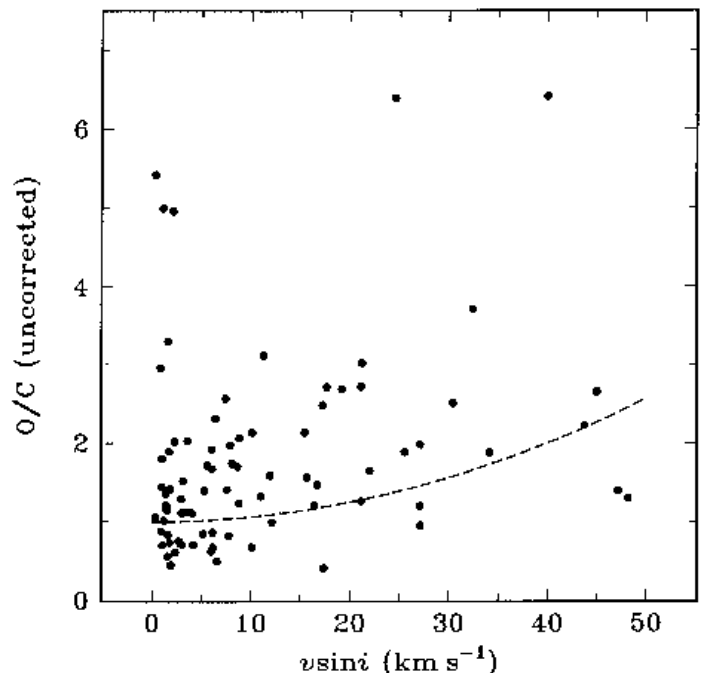
Fig. 10. The ratio of observed (O) to computed (C) velocity errors from the standard CORAVEL reductions vs. rotational velocity. Note the apparent absence of constant stars ($O/C < 1$) for $v \sin i > 15$ km s^{-1}. The dashed curve indicates our approximate correction factor to the computed error estimates. A few large O/C values are off scale

Table 2. Mean CORAVEL radial and rotational velocities (km s^{-1}) and derived parameters for 109 stars in the AHTC field of $20' \times 20'$ around NGC 3680. The remark "M" refers to data from Mermilliod et al. (1995), an asterisk to Sect. 3.5

Id no.	K no.	$\langle RV \rangle$	$\sigma_{\langle RV \rangle}$	n	σ_E	σ_C	O/C	$P(\chi^2)$	ΔRV	ΔT	$v\sin i$	$\sigma_{v\sin i}$	Remarks
1	1035	-4.96	2.10	5	13.30	2.71	3.21	0.000	35.9	763	40.0	10.0	*
2	1076	-8.27	0.31	3	0.35	0.52	0.66	0.661	0.9	420	6.2	4.5	
3	3006	11.86	0.36	5	0.81	0.47	1.68	0.024	2.0	2305	5.6	1.5	
4	1083	0.91	0.63	5	0.49	1.18	0.35	0.976	1.1	1968	17.4	2.5	
5	1194	-1.50	6.76	8	19.12	0.57	32.09	0.000	48.4	1591	7.6	1.7	
6	1207	0.37	0.52	5	0.96	0.80	0.83	0.622	2.2	1941	27.1	1.2	
7	1337	57.67	1.05	2	1.49	0.50	2.96	0.003	2.1	308	0.9	5.5	
8	1321	9.40	0.23	4	0.47	0.36	1.28	0.184	1.3	668	3.0	2.0	
9	1327	2.59	0.50	5	1.11	0.54	1.97	0.004	2.6	811	8.9	1.7	
10	1319	-1.01	1.16	8	1.73	1.34	0.53	0.968	6.3	1944	48.2	16.9	
11	1286	-0.27	0.20	8	0.57	0.30	1.89	0.001	1.7	3657	1.7	1.3	M*
13	1175	0.90	0.12	7	0.31	0.30	1.01	0.410	0.9	2981	1.2	1.6	M
14	1168	0.83	0.73	12	4.06	1.35	4.65	0.000	44.4	1565	24.5	12.8	*
15	1192	1.93	0.38	7	1.01	0.64	1.36	0.107	3.9	1541	15.7	1.1	
16	1197	37.87	7.11	6	17.42	0.90	18.64	0.000	42.5	1493	8.0	2.4	
17	1116	31.46	0.19	3	0.24	0.33	0.73	0.594	0.5	736	2.9		M
18	1176	-2.34	0.07	41	0.36	0.34	30.75	0.000	33.9	3000	2.3	0.8	M*
19	1208	0.41	1.14	7	3.01	1.60	1.09	0.372	9.8	1242	34.1		
20	1261	0.62	0.13	14	1.04	0.30	9.99	0.000	12.8	3769	1.3	1.2	M*
21	1306	11.04	0.36	4	0.72	0.47	1.51	0.081	1.8	421	3.2		*
21A	1304	1.58	0.57	4	1.14	0.44	2.48	0.000	2.4	1487	7.4	2.9	*
22	1318	1.32	0.26	11	1.28	0.90	35.23	0.000	84.3	1857	6.1	3.1	*
23	1310	0.67	0.58	6	1.42	0.43	3.29	0.000	4.2	1487	1.6	2.6	
24	1330	2.44	0.57	5	1.27	0.66	1.88	0.009	2.9	1968	6.1	3.0	
25	1348	2.15	0.61	7	1.61	0.75	2.01	0.001	4.0	1970	10.2	1.9	
25A	1331	-0.75	1.04	5	2.32	1.17	1.36	0.130	6.0	1215	27.1	2.1	
26	1374	0.32	0.11	8	0.31	0.29	1.06	0.358	0.9	3657	0.3	1.7	M
27	1404	0.83	0.46	10	1.45	0.29	4.99	0.000	4.5	3769	1.1		M*
29	1417	3.44	0.18	7	0.37	0.46	0.79	0.728	1.2	1966	7.8	1.3	
30	1396	1.57	0.90	5	1.94	0.91	1.86	0.011	4.8	1616	15.5	2.3	*
31	1405	8.24	1.01	4	2.03	0.76	2.18	0.003	4.3	671	19.2	1.9	
32	1454	1.37	0.98	5	2.20	0.81	2.27	0.001	5.5	1140	17.7	1.5	
33	1350	-0.93	1.89	9	5.67	0.60	8.16	0.000	14.1	1967	16.1	0.9	
34	1379	1.29	0.15	8	0.44	0.32	1.36	0.082	1.5	3297	1.4	1.6	M*
35	1376	0.61	0.33	5	0.66	0.67	0.91	0.525	1.6	1615	12.1	1.4	
36	1381	1.12	0.47	5	1.78	0.86	9.63	0.000	31.2	744	11.9		*
37	1395	2.18	0.76	7	2.01	1.06	1.34	0.116	6.5	1149	25.5	1.7	
38	1347	1.11	2.02	5	4.51	2.03	1.01	0.432	12.0	1541	43.7	4.7	*
39	1324	1.27	0.41	6	1.00	0.50	1.90	0.003	2.4	2284	7.9	8.4	
40	1334	-15.26	0.19	4	0.39	0.35	1.10	0.308	0.9	669	3.0		
41	1461	0.93	0.13	6	0.33	0.29	1.15	0.256	1.0	2982	1.5		M*
43	1510	2.71	0.80	6	1.93	1.19	1.27	0.183	4.9	2284	22.0	4.0	
44	1469	1.15	0.10	7	0.19	0.27	0.70	0.816	0.6	2962	1.1	1.4	M
45	1522	1.60	0.48	5	1.06	0.84	0.99	0.435	2.4	1476	21.1	2.2	
46	1507	2.00	0.46	5	1.02	0.78	1.24	0.198	2.9	1970	11.0	2.2	
46A	1524	7.43	1.64	5	3.67	1.46	1.59	0.041	9.4	835	30.4		
48	1640	-14.02	3.22	2	4.56	1.72	1.17	0.245	6.6	1546	45.0	5.0	
49	1653	67.45	9.37	4	18.74	0.56	32.41	0.000	43.2	663	7.9	2.1	
50	1781	50.70	0.18	7	0.48	0.40	1.21	0.213	51.3	2924	1.4		M
53	1873	0.64	0.12	7	0.23	0.32	0.73	0.782	0.8	2962	1.8	1.5	M
54	1899	16.54	0.50	7	1.31	0.24	5.42	0.000	3.2	2962	0.3		M
57	1661	33.85	4.04	2	3.33	2.39	0.58	0.566	5.0	62	47.1	7.2	
58	1638	34.01	19.28	3	33.39	0.79	38.49	0.000	64.8	363	12.7	2.5	
59	1643	-13.67	0.26	3	0.31	0.44	0.70	0.613	0.6	741	4.2	3.0	

We have tested this by plotting the individual, raw values of O/C as a function of $v\sin i$ (Fig. 10). For sharp-lined stars, one does observe the expected clustering of stars around the value $O/C = 1$, with a scattering of larger O/C values indicating true variability. For $v\sin i > 15-20$ km s^{-1}, however, the sample appears to consist exclusively of definite, but low-amplitude variables, an unlikely situation. We conclude that the standard CORAVEL reductions somewhat underestimate the velocity errors for rotating stars.

As a suitable, smooth correction function rising relatively steeply with $v\sin i$ as indicated by Fig. 10, we have chosen to "correct" the predicted errrors of a single velocity as computed by the standard CORAVEL reduction

Table 2. continued

Id no.	K no.	$<RV>$	$\sigma_{<RV>}$	n	σ_E	σ_C	O/C	$P(\chi^2)$	ΔRV	ΔT	$v\sin i$	$\sigma_{v\sin i}$	Remarks
60	1752	1.92	0.24	4	0.22	0.48	0.45	0.898	0.6	1086	1.9		
61	1755	12.08	0.58	4	1.17	0.50	2.25	0.002	2.7	423	6.4	3.0	
62(A)	1845	4.36	2.21	4	7.40	0.47	18.44	0.000	20.5	1122			*
63(B)	1910	-20.81	0.17	4	0.19	0.34	0.56	0.821	0.4	665	1.6		
64(C)	1891	-6.85	6.37	4	12.75	0.52	20.80	0.000	35.4	665	16.7	1.2	M
65(D)	1903	18.13	0.56	3	0.97	0.56	1.67	0.062	1.8	663	8.1	2.8	
66(E)	1984	32.16	2.83	4	5.67	0.38	14.85	0.000	11.4	742	4.5	1.7	
67(F)	1991	-0.31	0.32	4	0.63	0.57	1.09	0.317	1.4	664	4.1	2.8	
68(G)	1973	15.29	0.35	3	0.37	0.59	0.62	0.686	0.8	664	6.0	3.3	
70(I)	1050	1.41	0.30	4	0.59	0.41	1.45	0.104	1.3	700	1.0	3.1	
71(J)	1150	6.71	0.22	3	0.31	0.37	0.83	0.501	0.6	739	1.6	2.7	
74(N)	1639	1.41	0.32	5	0.45	0.67	0.63	0.808	1.1	1138	10.1	1.9	
76(P)	917	36.89	0.16	5	0.26	0.36	0.70	0.752	0.5	738	3.1	2.3	
77(Q)	1916	-7.24	0.46	3	0.79	0.64	1.18	0.248	1.5	358	8.8	2.6	
1079	1811	10.73	0.76	2	1.07	0.67	1.46	0.145	1.5	249	11.9	3.8	
1083	1699	3.52	0.41	3	0.71	0.51	1.39	0.147	1.3	771	1.6	4.9	
1085	1534	0.87	0.52	3	0.91	0.54	1.64	0.073	2.0	770	6.1	3.0	
1092	1458	7.01	0.27	3	0.46	0.41	1.12	0.293	1.0	380	3.4		
2032	1572	-14.32	0.54	1	0.52	0.52					6.9	4.3	
2040	1840	-15.84	0.51	1	0.51	0.51					2.2	6.9	
2062	1624	1.98	0.94	5	2.09	0.84	2.09	0.002	6.3	1119	17.3	1.5	
2076	2076	56.65	0.65	2	0.92	0.46	2.01	0.044	1.3	1118	2.3	4.8	
2085	1632	-1.39	0.25	3	0.36	0.42	0.83	0.510	0.7	770	5.2	2.5	
2093	1488	-10.51	1.84	2	2.60	0.52	4.95	0.000	3.7	247	2.1		
2094	1438	-7.21	6.62	2	9.36	0.51	17.66	0.000	13.9	252	7.5	4.2	
2095	1433	9.11	0.66	1	0.64	0.64					6.3	4.5	
2096	1411	-1.86	0.38	4	0.76	0.42	1.80	0.021	1.8	532	1.0	3.0	
2098	1447	32.29	0.35	2	0.24	0.47	0.49	0.627	0.3	1121	6.6	2.2	
2117	1852	-22.12	0.30	2	0.43	0.38	1.12	0.265	0.6	775	3.9		
2118	1800	0.59	0.26	4	0.44	0.51	0.84	0.556	1.0	1122	6.2	1.9	
2125	1678	12.06	0.58	2	0.82	0.59	1.37	0.171	1.2	1122	5.3	3.6	
3001	1353	3.62	0.41	6	1.01	0.69	1.25	0.178	2.9	1481	16.8	1.2	
3022	1265	-40.80	0.57	1	0.53	0.53					10.7	5.6	
3028	1031	52.49	0.60	1	0.59	0.59					4.6	4.7	
3040	1026	23.59	0.65	1	0.60	0.60					12.0	4.0	
3064	1097	-22.10	1.06	1	0.97	0.97					12.0	6.5	
3095	1008	1.07	2.99	2	4.23	1.40	2.36	0.019	6.0	1116	21.2	6.6	
3104	1203	56.65	0.25	2	0.22	0.36	0.61	0.542	0.3	1111	2.4		
3105	1204	6.00	0.49	1	0.48	0.48					5.6		
3113	1362	124.39	0.51	1	0.51	0.51					4.4	4.9	
4002	1373	0.16	1.47	6	3.60	0.97	2.24	0.000	10.8	1472	32.4	1.8	
4011	1181	63.06	0.50	1	0.50	0.50					3.8	4.9	
4015	1127	25.86	0.30	2	0.32	0.43	0.75	0.452	0.5	401	2.7	3.1	
4027	925	-15.57	0.40	3	0.70	0.50	1.36	0.158	1.3	398	7.6	2.1	
4028	936	0.96	0.65	6	1.04	1.10	0.65	0.839	2.8	1156	27.1	2.2	
4081	952	-0.08	0.71	5	1.60	0.51	2.89	0.000	4.0	811	11.2	1.3	
4088	1045	9.49	0.35	2	0.44	0.50	0.88	0.379	0.6	95	0.9	4.5	
4094	1164	-0.18	0.19	5	0.43	0.31	1.41	0.096	1.3	779	1.9		M*
4106	1268	-9.68	0.51	3	0.88	0.73	1.04	0.357	1.7	402	16.4	1.7	
4114	1133	1.78	0.47	4	0.94	0.55	1.63	0.050	1.8	776	8.6	2.0	
4116	1084	33.25	0.61	1	0.60	0.60					3.4	5.5	
4121	967	4.56	1.51	3	2.61	0.96	2.12	0.012	5.2	379	21.1	2.4	
4140	1357	17.63	0.84	2	1.18	0.58	2.02	0.044	1.7	95	3.6	3.8	
6028		2.29	0.20	5	0.94	0.83	13.92	0.000	31.4	668	21.0		*
7020		48.30	0.40	1	0.39	0.39					3.0		

(σ_C in Table 2) by a factor of $(1 + (v\sin i\ /40)^2)$. In other words, we increase the raw σ_C by a quadratic factor which doubles the estimated value of σ_C by $v\sin i\ = 40$ km s^{-1}. This procedure effectively amounts to dividing the raw O/C values shown in Fig. 10 by the curve shown in the same fiure and yields the revised O/C values given in Table 2. We have also applied this factor before computing

the values of χ^2 given in Table 2 and used in judging the constancy or otherwise of the radial velocity.

In computing the standard error estimates for the *mean* velocities given in Table 2, we have taken into account the values of σ_C as well as the dispersion among the individual velocities (σ_C). Thus, fortuitously close agreement between a few observations ($O/C < 1$) will not lead

to an unduly sanguine view of the accuracy of their mean (cf. also Andersen & Nordström 1983).

For spectroscopic binaries, the mean velocity given in Table 2 has been computed from the available observations and thus appears with fairly large errors. Ideally, their full spectroscopic orbits should be determined. Obtaining the necessary 15-25 radial-velocity observations per star distributed over several years is, however, a major task and beyond the primary goal of this study, since binaries will be excluded from the isochrone fits in any case. For double-lined binaries (SB2), the systemic velocity (with errors, plus the mass ratio) can be computed with good accuracy by the method of Wilson (1941) and is then given in Table 2 instead of a simple mean.

5. Conclusions

With the data in this paper, NGC 3680 has been brought to a degree of completeness in both photometry, radial velocities, and proper motions previously reserved for a handful of standard clusters such as the Hyades, Pleiades, and a very few more. These data allow a fairly complete discussion of the cluster's membership, constraints on theoretical isochrones imposed by the CMD, age, and dynamical state. These topics are the subject of Paper II in this series (Nordström et al. 1996).

References

Andersen J., Andersen M.I., Klougart J., et al., 1995a, ESO Messenger 79, 12

Andersen J., Nordström B., Ardeberg A., et al., 1985, A&AS 59, 15

Andersen J., Nordström B., 1983, A&A 122, 23

Andersen J., Nordström B., 1991, in: The Formation and Evolution of Star Clusters, Janes K. (ed.), ASPC 13, p. 357

Andersen M.I., Storm J., Freyhammer L.M., 1995b, in: Understanding and Calibrating HST and ESO Instruments, Benvenuti P., (ed.), p. 87

Anthony-Twarog B.J., Heim E.A., Twarog B.A., Caldwell N., 1991, AJ 102, 1056 (AHTC)

Anthony-Twarog B.J., Twarog B.A., Shodhan S., 1989, AJ 98, 1634 (ATTS)

Baranne A., Mayor M., Poncet J.-L., 1979, Vistas. Astron. 23, 279

Benz W., Mayor M., 1981, A&A 93, 235

Benz W., Mayor M., 1984, A&A 138, 183

Crawford D.L., Perry C.L., 1966, AJ 71, 206

Daniel S.A., Latham D.W., Mathieu R.L., Twarog B.A., 1994, PASP 106, 281

Demarque P., Sarajedini A., Guo X.-J., 1994, ApJ 426, 165

Duquennoy A., Mayor M., 1991, A&A 248, 485

Eggen O.J., 1969, ApJ 155, 439 (EG)

Grønbech B., Olsen E.H., Strömgren B., 1976, A&AS 26, 155

Janes K.A., Phelps R.L., 1994, AJ 108, 1773

Kozhurina-Platais V., Girard T.M., Platais I., van Altena W.F., 1995, AJ 109, 672

Lasker B.M., Sturch C.R., McLean B.J., Russel J.L., Jenkner H., Shara M.M., 1990, The Guide Star Catalog. I. Astronomical and Algorithmic Foundations, AJ 99, 2019

Mathieu R.D., Latham D.W., 1986, AJ 92, 1364

Mathieu R.D., Latham D.W., Griffin R.F., Gunn J.E., 1986, AJ 92, 1100

Mayor M., 1985, in: Stellar Radial Velocities, Philip A.G.D., Latham D.W. (eds.) IAU Colloq. No. 88. L. Davis Press, Schenectady, p. 35

Mayor M., Maurice E., 1985, in: Stellar Radial Velocities, Philip A.G.D., Latham D.W. (eds.) IAU Colloq. No. 88. L. Davis Press, Schenectady, p. 299

Mermilliod J.-C., Andersen J., Nordström B., Mayor M., 1995, A&A 299, 53

Nissen P.E., 1988, A&A 199, 146 (N88)

Nissen P.E., Crawford D.L., Twarog B.A., 1987, AJ 93, 634

Nordström B., Andersen J., 1991, ESO Messenger 63, 34

Nordström B., Andersen J., Andersen M.I., 1996, A&A, (Paper II) (to be submitted)

Stetson P.B., 1987, PASP 99, 191

VandenBerg D.A., 1983, ApJS 51, 29

VandenBerg D.A., 1985, ApJS 58, 711

Wilson O.C., 1941, ApJ 93, 29